Supporting Information

Symmetry Related $[Ln^{III}_{6}Mn^{III}_{12}]$ Clusters towards Single-Molecule Magnets and Cryogenic Magnetic Refrigerants

Jun-Liang Liu,[†] Wei-Quan Lin,[†] Yan-Cong Chen,[†] Ji-Dong Leng,[†] Fu-Sheng Guo,[†] Ming-Liang Tong*[†]

[†] *Key Laboratory of Bioinorganic and Synthetic Chemistry of Ministry of Education, State Key Laboratory of Optoelectronic Materials and Technologies, School of Chemistry & Chemical Engineering, Sun Yat-Sen University, Guangzhou, 510275, P. R. China. Fax: (+)86 20 8411-2245; E-mail: tongml@mail.sysu.edu.cn*

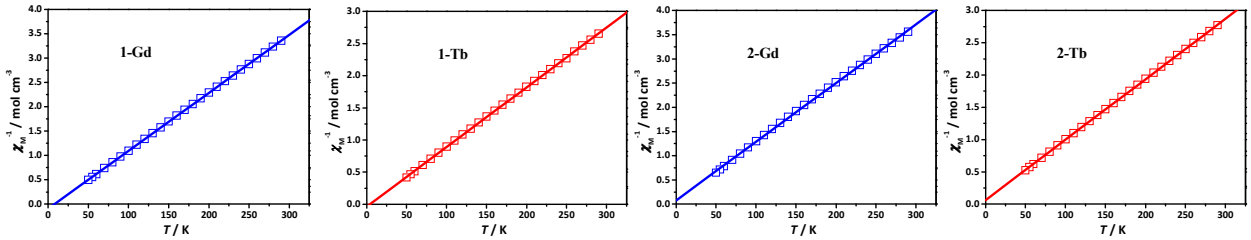

Figure S1. The fitting of the experimental data to a Curie-Weiss law from 50 K to 290 K for **1** and **2**.

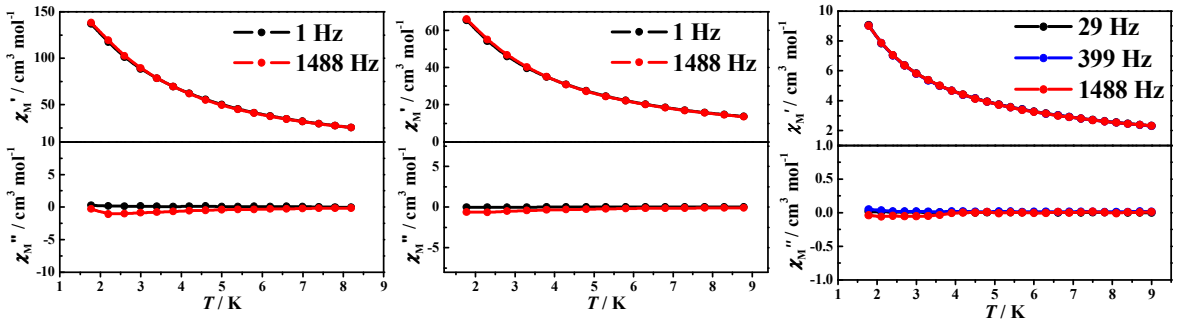

Figure S2. Plot of ac susceptibility vs. temperature for **1-Gd** (*left*), **2-Gd** (*middle*) and **2-Y** (*right*) at H_{ac} = 5 Oe and H_{dc} = 0.

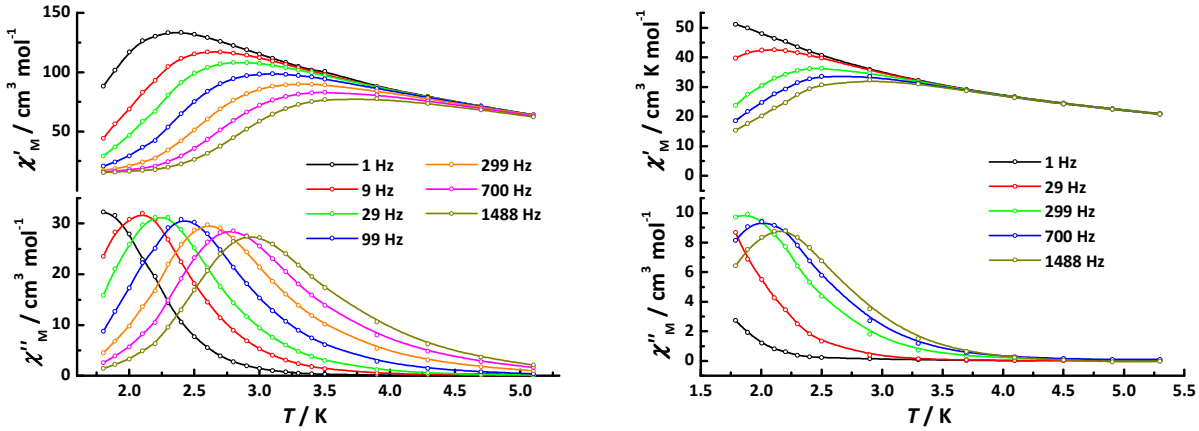

Figure S3. Plots of ac susceptibility vs.temperature for **1-Tb** (*left*) and **2-Tb** (*right*) oscillating at 1–1488 Hz at H_{ac} = 5 Oe and H_{dc} = 0.

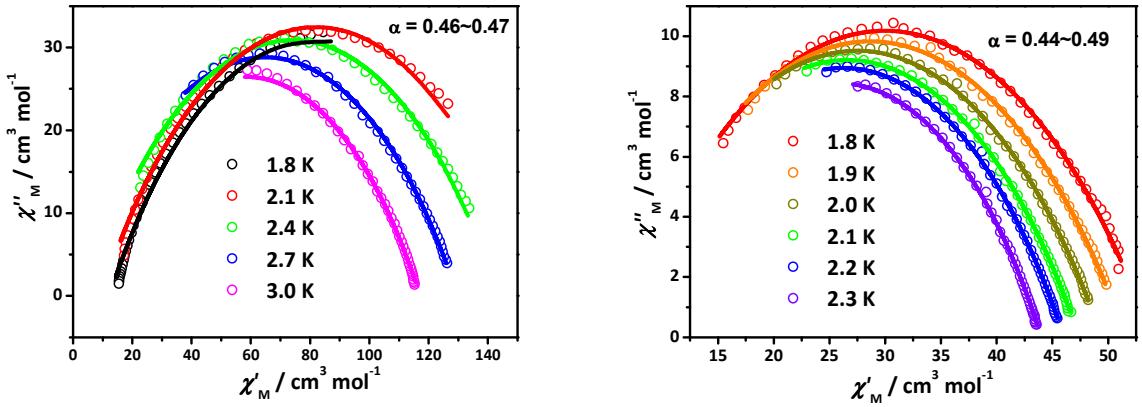

Figure S4. Cole-Cole plots for **1-Tb** (*left*) and **2-Tb** (*right*), obtained from variable-frequency ac susceptibility data under a zero dc field in the temperature range. Solid lines represent fits to the data using a generalized Debye model.

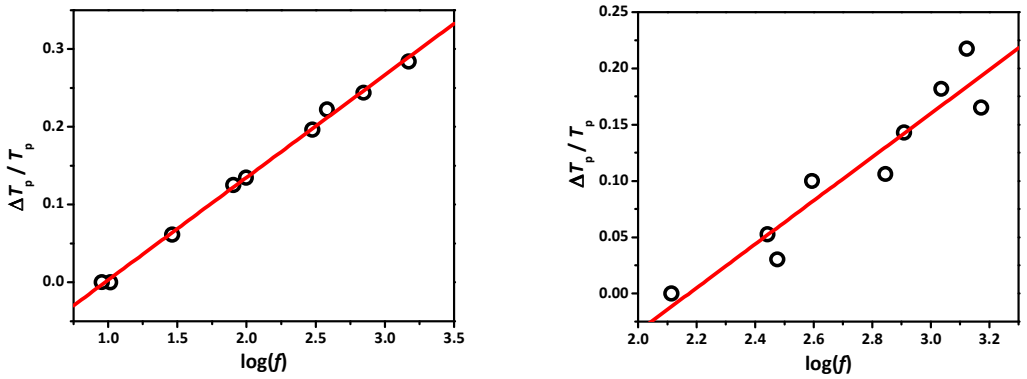

Figure S5. The log(f) vs. $\Delta T_p/T_p$ plots for **1-Tb** (*left*) and **2-Tb** (*right*). The value of φ can be extracted from the slope.

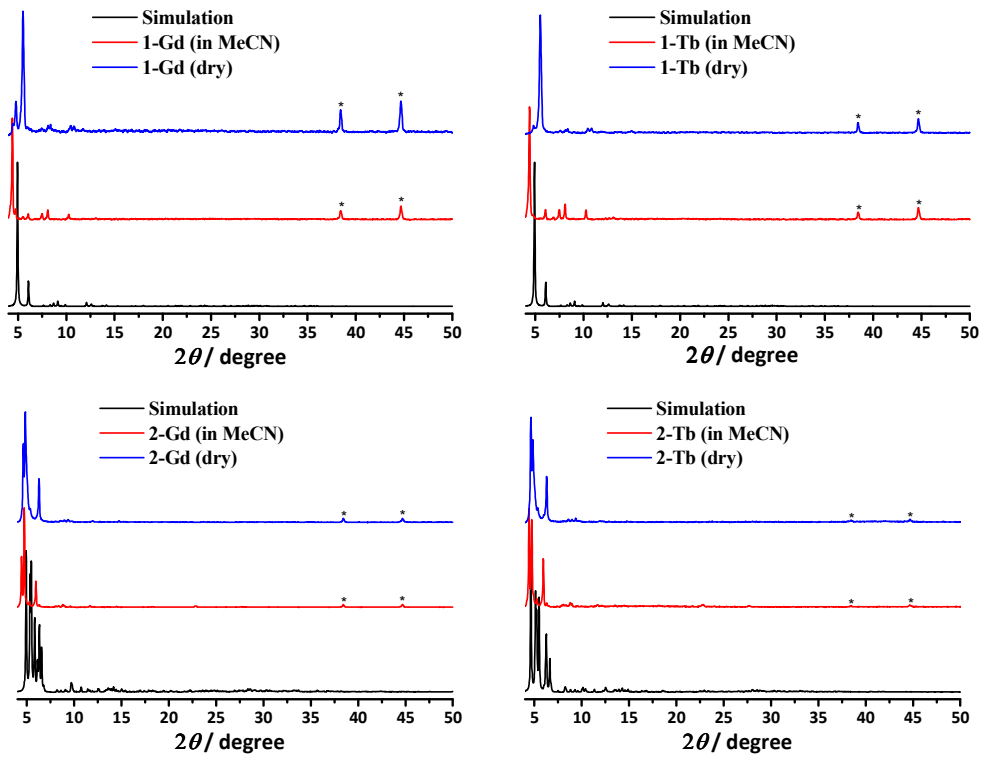

Figure S6. The experimental X-ray Powder diffraction (XRPD) patterns and the simulated ones. The peaks marked with * were due to silicon carrier. The samples are measured in MeCN or under air ambient. The difference between them indicate that the content of the solvent molecules shift the diffraction angles.

Table S1. Bond valence sum calculations of Mn and Ln oxidation states in the crystal structures of **1** and **2**.

Complex **1-Gd**			
Gd1	3.298(19)	Gd2	2.938(18)
	+2	**+3**	**+4**
Mn1	3.561(23)	3.284(21)	3.222(21)
Mn2	3.417(27)	3.183(25)	3.109(24)
Mn3	3.461(31)	3.223(29)	3.149(28)

Complex **2-Gd**			
Gd1	3.257(34)	Gd2	2.998(30)
Gd3	3.222(33)	Gd4	3.161(36)
Gd5	2.957(32)	Gd6	3.062(35)
	+2	**+3**	**+4**
Mn1	3.516(56)	3.277(53)	3.200(51)
Mn2	3.324(57)	3.097(53)	3.025(52)
Mn3	3.459(52)	3.222(49)	3.147(48)
Mn4	3.398(49)	3.165(46)	3.092(45)
Mn5	3.269(42)	3.015(39)	2.958(38)
Mn6	3.172(42)	2.925(39)	2.870(38)
Mn7	3.316(42)	3.057(39)	3.000(38)
Mn8	3.234(43)	2.982(39)	2.926(38)
Mn9	3.399(50)	3.169(46)	3.094(45)
Mn10	3.468(57)	3.230(54)	3.155(52)
Mn11	3.356(47)	3.127(44)	3.054(43)
Mn12	3.380(55)	3.147(52)	3.075(50)

Complex **1-Tb**			
Tb1	3.041(17)	Tb2	2.758(16)
	+2	**+3**	**+4**
Mn1	3.560(22)	3.283(20)	3.222(20)
Mn2	3.456(26)	3.219(24)	3.144(24)
Mn3	3.465(30)	3.228(28)	3.153(27)

Complex **2-Tb**			
Tb1	3.149(18)	Tb2	2.950(16)
Tb3	3.153(19)	Tb4	3.127(18)
Tb5	2.953(18)	Tb6	3.057(18)
	+2	**+3**	**+4**
Mn1	3.298(24)	3.041(22)	2.984(21)
Mn2	3.347(24)	3.086(22)	3.028(22)
Mn3	3.323(24)	3.064(22)	3.007(22)
Mn4	3.301(23)	3.044(21)	2.987(21)
Mn5	3.469(26)	3.232(25)	3.157(24)
Mn6	3.477(27)	3.238(25)	3.163(24)
Mn7	3.492(27)	3.252(25)	3.177(25)
Mn8	3.466(31)	3.230(29)	3.155(28)
Mn9	3.529(30)	3.288(28)	3.211(27)
Mn10	3.428(28)	3.193(26)	3.119(26)
Mn11	3.417(26)	3.181(25)	3.108(24)
Mn12	3.476(26)	3.238(24)	3.163(24)